Pramana – J. Phys. (2018) 90:41
https://doi.org/10.1007/s12043-018-1527-z

Activation cross-section data for α-particle-induced nuclear reactions on natural vanadium for practical applications

B M ALI[1], M AL-ABYAD[1,*], U SEDDIK[1], S U EL-KAMEESY[2], F DITRÓI[3], S TAKÁCS[3] and F TÁRKÁNYI[3]

[1]Physics Department (Cyclotron Facility), Nuclear Research Centre, Atomic Energy Authority, Cairo 13759, Egypt
[2]Physics Department, Faculty of Science, Ain Shams University, Cairo, Egypt
[3]Institute for Nuclear Research (ATOMKI), Hungarian Academy of Sciences, Debrecen 4026, Hungary
*Corresponding author. E-mail: alabyad_m@yahoo.com

MS received 8 May 2017; revised 15 September 2017; accepted 12 October 2017;
published online 20 February 2018

Abstract. Excitation functions for α-induced reactions on natural vanadium were measured in the energy range up to 20 MeV. The stacked-foil activation technique was used. The experimental results were compared with the theoretical calculations using EMPIRE-3.1, EMPIRE-3.2.2 and TENDL 2015, and with earlier experimental results. Thick target yields were calculated for the production of ^{54}Mn and for the associated impurity ^{52}Mn.

Keywords. ^{4}He beam; α-particles; ^{nat}V; induced nuclear reaction; ^{54}Mn; ^{52}Mn; cross-section; excitation function; stacked-foil technique; integral yield.

PACS No. 25.55.−e

1. Introduction

The radioisotope ^{52g}Mn with $T_{1/2} = 5.6$ d decays for 70.4% electron capture (EC) + 29.6% β^+. Its decay data indicate that this nuclide is convenient for radiotracer studies, mainly for positron emission tomography (PET). It can facilitate *in vivo* studies that utilise manganese as a radiotracer for antibodies, nanoparticles, etc. or as a means to image the biodistribution of manganese cations [1]. The longer-lived ^{54}Mn ($T_{1/2} = 312.2$ d) decays for 100% EC through a single γ-line of 834.8 keV energy to the stable ^{54}Cr. This γ emitter is used as a radiotracer for studying manganese toxicity, manganese metabolism [2] and for understanding the functioning and development of the brain [3–5]. The production of ^{54}Mn with high precision is also useful for thin layer activation (TLA) analysis.

The main roots of ^{54}Mn production are the reactions ^{54}Fe(n,p)^{54}Mn and ^{55}Mn(n,2n)^{54}Mn using nuclear reactors. These reactions produce ^{54}Mn in good yield. The early studies relevant to the production of ^{54}Mn utilising accelerators were concentrated on proton- or deuteron-induced nuclear reactions in iron, chromium and manganese [1,6–10] or α-induced nuclear reactions in chromium and vanadium [11–26]. Reports on cross-section data of vanadium targets, for the reaction ^{51}V(α,n)^{54}Mn are numerous. However, almost all these data were used to study the (α,n) reaction mechanism and to compare it with some nuclear reaction codes. A few researchers reported experimental thick target yields for ^{51}V(α,n)^{54}Mn solely without cross-section data mainly for medical applications [27,28].

In this study, we introduced α-particle-induced nuclear reactions on natural vanadium up to 20 MeV. It should be mentioned that this study represents a part of (a supplement) systematical study of charged particles-induced nuclear reactions. Earlier studies were on vanadium activation with deuterium [29] and ^{3}He particles [30]. We studied the excitation function of ^{51}V(α,n)^{54}Mn primarily and, the excitation function of ^{50}V(α,2n)^{52}Mn. Natural vanadium exists as two isotopes; the first is ^{51}V with abundance of 99.75% and the second is the very long-lived ^{50}V ($T_{1/2} = 2.1 * 10^{17}$ yr) with only 0.25% abundance.

2. Experimental set-up

The excitation function of α-induced reactions on natural vanadium was measured using the stacked-foil activation technique and γ-ray spectrometry. Irradiation was carried out at the MGC-20E cyclotron of the Institute for Nuclear Research (ATOMKI), Debrecen,

Table 1. Contributing reactions kinematics (taken from [35]).

Product	Contributing reactions	Q-Value (MeV)	Threshold energy E_{th} (MeV)
^{54}Mn	^{51}V(α,n)	−2.3	2.5
^{52}Mn	^{50}V(α,2n)	−12.2	13.2
	^{51}V(α,3n)	−23.3	25.1

Hungary. Using external α-particle beam of 20 MeV, irradiation took place at a constant beam current of 108 nA for about 80 min. The energy and intensity of the extracted beam was derived from the accelerator setting. The incident energy was determined online using a fully automated system [31]. For current measurement, the target stack was irradiated in a Faraday cup target holder, with a beam collimator and a secondary electron suppresser. The effective beam diameter on the target was about 7 mm. The target assembly consisted of nine high-purity (>99.98%; supplied by Goodfellow) natural vanadium foils (thickness: 8.41 μm) sandwiched with three high-purity natural Ti monitor foils of 12 μm thickness.

The monitor foils were mainly used for the exact determination of the beam intensity and energy by taking into account the comparison of the re-measured excitation function of ^{nat}Ti(α,x)^{51}Cr reaction, over the studied energy domain with the recommended values in the updated version of IAEA-TECDOC 1211 [32]. They also serve as projectile energy degraders. The energy degradation along the stack was calculated using the code SRIM-2013 based on Ziegler's polynomial approximations for the stopping power of energetic charged particles in all elements [33]. The incident energy at the middle of the first foil was estimated to be 19.5 MeV. This is the average value between the entrance and departure energies from the first foil. The uncertainty on the median energy increases along the stack from 0.2 MeV in the first foil up to 0.7 MeV in the last foil due to uncertainty on the primary incident energy, uncertainty on the thickness of target foils and energy straggling.

Without chemical separation, the activity of the produced radionuclides was measured using HPGe detectors of high resolution (2 keV at the 1333 keV γ-ray peak) coupled to acquisition/analysis software. Their efficiencies were calculated experimentally with the standard sources ^{152}Eu and ^{133}Ba for different distances ranging between 6 and 20 cm. Measurements of the induced activity started in the same day of irradiation. The second activity measurement was done over 1–4 days after the end of bombardment (EOB). After two weeks, longer measurements (12–24 h) started to achieve good counting statistics. Spectra analyses were done using the program FGM [34].

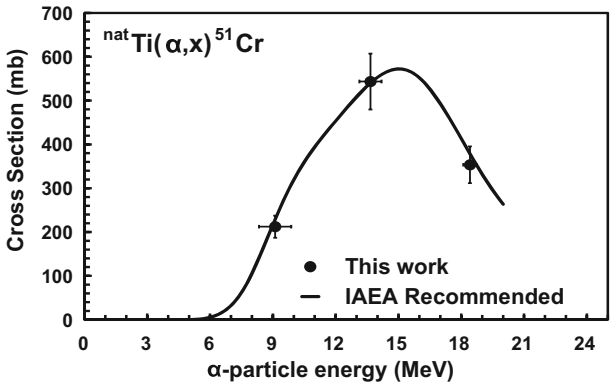

Figure 1. Present versus recommended excitation function of the monitor reaction ^{nat}Ti(α,x)^{51}Cr.

The cross-sections were calculated using the well-known activation formula from the observed activities of the product nuclei, beam and target parameters. The two reported cross-section data represent isotopic cross-sections and thus the data have been extrapolated to 100% enrichment for each reaction.

Decay data of the products and contributing reaction kinematics were taken from [35]. The contributing reaction kinematics are given in table 1. Comparison between excitation function of the monitor reaction ^{nat}Ti(α,x)^{51}Cr and the recommended data of the IAEA-TECDOC 1211 [32] is shown in figure 1.

The total uncertainty on the cross-section values was evaluated in the same way as in many previous publications in the standard way [36], by taking the square root of the sum of the square of all individual contributions. Uncertainties involved in the calculations are counting statistics (1–12%), effective target thickness (5%), beam current (7%), detector efficiency (7%) and decay data (3%). The total determined uncertainties were about 12–17%.

3. Model calculations

Theoretical calculations of the excitation functions were performed using two familiar nuclear models: EMPIRE (two versions 3.1 and 3.2.2) [37,38] and TALYS-1.6 [39]. Both of them include several nuclear reaction codes and nuclear data libraries in their model systems. A brief description of the EMPIRE-3.1, TALYS-1.6

models and the involved nuclear codes can be seen in [40–42]. EMPIRE-3.2.2 (Malta) is a new version that can be installed in windows XP or higher versions. The code contains various models for nuclear reaction mechanisms, level densities and optical models. Pre-equilibrium processes were calculated using the phenomenological exciton model PCROSS with mean free path parameter values $K_{\mathrm{mfp}} = 0$, 1.05, 1.5 and 2. The nuclear level densities in EMPIRE-3.2.2 code are described by four different models. Three models are phenomenological: Enhanced generalised superfluid model (EGSM), generalised superfluid model (GSM) and Gilbert–Cameron model (GCM). The fourth model is based on Hartree–Fock–Bogoliubov microscopic model (HFBM). The four models are already included in the reference input parameter library (RIPL-3) [43]. The following parameters also are included in the RIPL-3: nuclear masses, ground-state deformations, nuclear levels and their characteristics, gamma strength functions, fission barriers and optical model parameters. Various local and global optical model parameters (OMP) were found in the RIPL-3. Different sets of parameters were used in our cross-section calculations. TALYS theoretical data represent the library TENDL 2015 which is based on default and adjusted TALYS-1.6 calculations [44]. A recommended curve for the excitation function of ^{51}V(α,n)^{54}Mn was constructed by data fitting of the present and literature cross-section data.

4. Results and discussion

The excitation functions for ^{51}V(α,n)^{54}Mn- and ^{50}V(α,2n)^{52}Mn-induced nuclear reactions were measured from their respective threshold up to 20 MeV. Each radionuclide was identified by its characteristic γ-rays (mentioned in the text). The measured cross-section values and their uncertainties are presented in table 2. The present experimental cross-section data are shown in figures 2–6 together with the experimental results in the literature and the theoretical calculations.

Table 2. Cross-section values and uncertainties for the ^{54}Mn and ^{52}Mn production.

Mean energy (MeV)	Cross-section (mb)	
	^{54}Mn	^{52}Mn
19.5±0.3	196±24	378±55
17.3±0.4	363±42	251±40
16.2±0.4	488±57	180±28
15.0±0.5	626±73	78±13
12.3±0.6	623±72	
10.8±0.7	505±58	
7.2±0.9	42±5	
4.9±1.0	3±0.5	

4.1 $^{51}V(\alpha,n)^{54}Mn$ reaction

The cross-section is totally isotopic and the reaction is the pure (α,n) reaction. The cross-section dataset represents direct cross-section as there is no cumulative contribution. Cross-section measurements were performed using the single line in ^{54}Mn decay scheme ($E_\gamma = 834.8$ keV, $I_\gamma = 99.976\%$). The excitation function increases up to a maximum value at 12–15 MeV. Its experimental threshold at 5 MeV is in correspondence with the (α,n) channel threshold energy at 2.5 MeV. Figure 2 shows a comparison between our experimental data and the data found in the literature as well as theoretical EMPIRE-3.1 and TENDL 2015 calculations.

The overall trend of all experimental data is a high-energy tail following a peak. The data in the rising and tail parts are in agreement with each other, while the data in the peak region are fairly more scattered. Almost all errors are due to uncertainty in energy determination in the stacks because of the higher energy of incoming α-particles. Accordingly, these scattered data points correspond to the foils at the end of their stacks. The only exceptions are the data of [13,23]. These data show shifts towards lower and higher energies respectively.

The data in [13,15,20] built up the rising part of the excitation function. These data are consistent with each other and with the other experiments except the high-energy part of Vlieks *et al* [13]. It shows a shift towards lower energies and displays a cross-section value higher than other experiments by about 30%.

Measurements by Iguchi *et al* [11] covered the energy range 30 MeV→7 MeV. Their data are consistent with the other experimental data except for one point at 7 MeV which shifted towards low energies by about 2 MeV. Bowman and Blann covered the energy range 85 MeV–7 MeV [12]. Their data are more or less in agreement with other data especially in the high-energy range. In the low-energy range two cross-section points, that correspond to the last two foils in the stack, show more scattering than other data.

The data reported in [14,24] covered the high-energy tail of the excitation function. Their data are in good agreement with each other and with the overall excitation function.

The experimental data in [16,19,22] are in good agreement with each other. These data are also consistent with the other experiments except at one point for each. These points correspond to the last foil in each stack. In Singh *et al* [22] measurements, we observed that the displayed data in EXFOR database are actually about ten

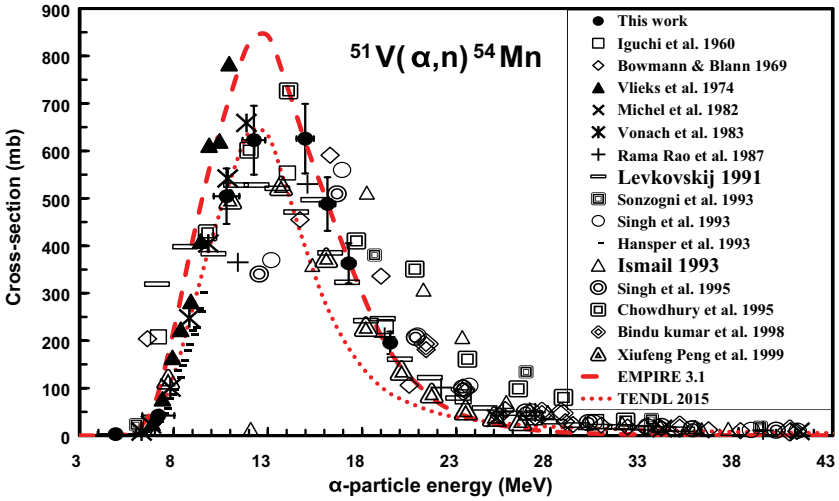

Figure 2. Experimental and theoretical excitation functions of ^{51}V(α,n)^{54}Mn nuclear reaction.

times larger than other experimental data. In their original paper, the authors introduced this reaction in two figures. The first one displayed lots of excitation functions. The second figure displayed only the ^{51}V(α,n) reaction. The data in the first figure are about ten times the data of the second. EXFOR data are taken from the first figure (the wrong one) while, we postulated the data in the second one as the right data.

Measurements by Levkovskij [17] are consistent with the other experimental results in the high-energy tail. Levkovskij data in the rising part and peak region are somewhat scattered. Sonzogni *et al* experimental data [18] covered a wide energy range (85 MeV–6 MeV). The first cross-section point at 6 MeV shows a shift towards lower energy, while all other data show a shift towards high energies. The data reported in [21] are not consistent with the other experiments. These data show a shift towards high energies.

Chowdhury *et al* [23] results are consistent with other results in the rising part of the excitation function, while the data in the high-energy tail show a shift towards high energies. Their maximum reported value is higher than other experiments by about 15%. One data point by Peng *et al* [25] in the peak region is lower than other experiments by about 15%. The remaining points measured by Peng *et al* [25] are in good agreement with other experimental data.

The results of theoretical calculations using EMPIRE-3.1 and TENDL have the same trend as that of the experimental excitation function. EMPIRE-3.1 code data match more or less with the experimental data in the tail region while overestimating them in both rising and peak regions. TENDL library calculations reproduce the rising part of the experimental data while they underestimate the tail region.

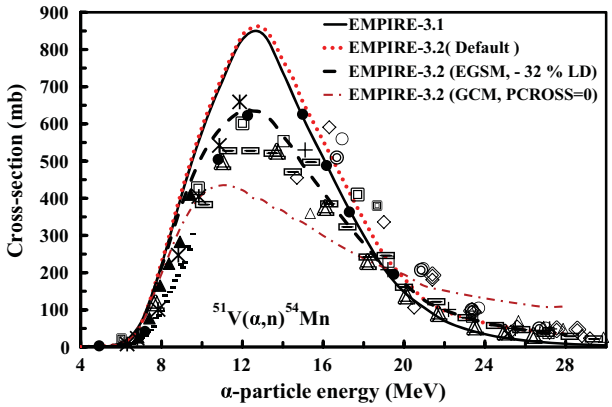

Figure 3. Comparison between selected experimental (markers) and theoretical excitation functions (lines) based on EMPIRE-3.1 and EMPIRE-3.2.2 calculations of ^{51}V(α,n)^{54}Mn reaction.

Calculation of the nuclear reaction cross-section of this reaction was also performed using the code EMPIRE-3.2.2 (figure 3) up to 28 MeV. This figure displays a comparison between the theoretical EMPIRE-3.2.2 calculations and selected experimental data. The selected data points represent consistent data from different groups. In EMPIRE-3.2 calculations, various combinations between the level density models and PCROSS mean free path values (K_{mfp} = 0, 1.05, 1.5 and 2) were used. For all level density models, regardless of the mean free path value, EMPIRE-3.2 excitation functions match with that calculated by EMPIRE-3.1 (default parameters) except for the GCM model. Using GCM level density model with different mean free path values result in lower cross-section values than those calculated by other models. During

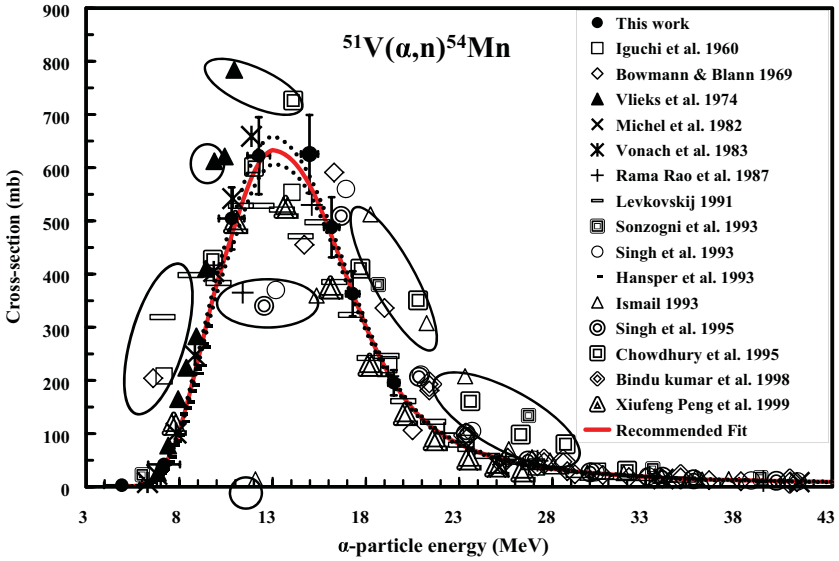

Figure 4. Comparison between experimental data and the recommended fit of ^{51}V(α,n)^{54}Mn excitation function. The black dotted lines are the 95% confidence of the fitting curve.

calculations, we noted that increasing the mean free path value does not affect the calculated excitation functions at rising and peak regions. There were only small variations at the high-energy tails. Using the EGSM model for nuclear level density description regardless of the mean free path value, the calculated excitation function matches the experimental data with an energy shift about 1 MeV if the level density parameter is reduced by 32%.

So, theoretical calculations predict only the shape of the excitation function with different magnitudes. For good prediction of both shape and magnitude, we estimated best fit of the experimental data using the commercially available program table curve-2d [45]. Experimental data were inserted to the program, then a polynomial and rational fitting started. The data points beyond the 3σ limits were neglected during fitting procedure. Also the scattered data points that have high deviations were discarded as they disturb the fitting process. The recommended fitting and its 95% confidence limits of excitation function are shown in figure 4 together with the experimental data. The encircled data represent the data neglected during fitting process. Numerical values of the recommended cross-section data and their 95% confidence limits are given in table 3. A comparison between the recommended curve and theoretical EMPIRE-3.2 calculations (using EGSM level density model and decreasing level density parameter by 32%) as well as the selected experimental data are given in figure 5.

4.2 $^{50}V(\alpha,2n)^{52}Mn$ reaction

There are three intense γ-lines in its decay scheme (E_γ = 744.2 keV, I_γ = 90%), (E_γ = 935.5 keV, I_γ = 94.5%) and (E_γ = 1434.1 keV, I_γ = 100%). These γ-lines were used in the cross-section measurements. Again the cross-section is totally isotopic and the reaction is pure (α,2n). The cross-section dataset represents cumulative data because of a small contribution from the isomeric transition (^{52m}Mn, $T_{1/2}$ = 21.2 min, 1.75% IT). Consequently, evaluation of the concerned ground state was started after the total decay of its isomeric state.

As the whole contribution of the excitation function in our energy range comes only from the low abundance of ^{50}V, low cross-section values were expected for this reaction. So, we normalised our cross-section data to 100% enrichment of ^{50}V. As seen from table 1, at energies >25 MeV, the channel ^{51}V(α,3n) starts to contribute and it governs the excitation function to the extent that (α,2n) channel contribution can be neglected. The excitation function increased from 78 mb at about 15 MeV to 378 mb at the end of our energy range (figure 6). One dataset of Xuifeng Peng *et al* is found in the literature for this reaction [25]. Their results are in good agreement with ours and reveal a peak around 22 MeV out of our energy range.

The theoretical data based on TENDL 2015 match the experimental excitation function in shape and magnitude up to about 18 MeV, then underestimate

Table 3. Recommended cross-section data for the $^{51}V(\alpha,n)^{54}Mn$ reaction.

E (MeV)	σ (mb)	95% Conf. limit		E (MeV)	σ (mb)	95% Conf. limit		E (MeV)	σ (mb)	95% Conf. limit	
		Upper	Lower			Upper	Lower			Upper	Lower
5	0.26	0.23	0.29	15	566.1	549.6	582.6	27	38.7	37.6	39.8
5.5	1.16	1.10	1.22	15.5	529.1	514.1	544.1	27.5	36.0	34.9	37.0
6	4.2	4.0	4.4	16	486.2	472.2	500.1	28	33.5	32.5	34.6
6.5	12.2	11.8	12.7	16.5	439.6	426.8	452.4	28.5	31.4	30.5	32.4
7	29.5	28.3	30.7	17	391.9	380.5	403.3	29	29.6	28.6	30.5
7.5	60.1	57.5	62.7	17.5	345.3	335.4	355.1	29.5	27.9	27.0	28.8
8	106.7	102.0	111.4	18	301.4	293.1	309.7	30	26.4	25.5	27.3
8.5	167.9	160.6	175.2	18.5	261.6	254.6	268.5	30.5	25.1	24.2	25.9
9	238.6	228.6	248.6	19	226.2	220.3	232.0	31	23.7	22.8	24.6
9.5	311.4	298.2	324.6	19.5	195.5	190.5	200.6	31.5	22.5	21.6	23.4
10	379.8	362.6	396.9	20	169.4	164.9	173.8	32	21.2	20.4	22.1
10.5	440.0	418.6	461.5	20.5	147.3	143.4	151.2	32.5	20.1	19.2	20.9
11	492.5	467.5	517.4	21	128.9	125.4	132.3	33	18.9	18.1	19.7
11.5	547.3	520.1	574.6	21.5	113.5	110.3	116.6	33.5	17.9	17.1	18.6
12	591.1	563.3	618.9	22	100.6	97.8	103.4	34	16.9	16.1	17.6
12.3	610.5	582.9	638.1	22.5	89.7	87.2	92.2	34.5	16.0	15.3	16.7
12.5	620.2	592.9	647.5	23	80.5	78.3	82.8	35	15.2	14.5	15.9
12.8	629.8	603.1	656.6	23.5	72.6	70.6	74.6	35.5	14.5	13.8	15.3
13	633.0	606.8	659.2	24	65.7	63.9	67.6	36	14.0	13.2	14.7
13.2	631.7	606.2	657.2	24.5	59.7	58.1	61.3	36.5	13.5	12.7	14.3
13.5	627.8	603.6	652.0	25	54.4	53.0	55.8	37	13.1	12.3	13.8
13.8	621.4	598.7	644.1	25.5	49.7	48.4	51.0	37.5	12.7	12.0	13.4
14	615.6	594.0	637.2	26	45.6	44.4	46.8	38	12.4	11.7	13.0
14.5	595.2	576.4	614.0	26.5	41.9	40.8	43.1	38.5	12.0	11.4	12.6

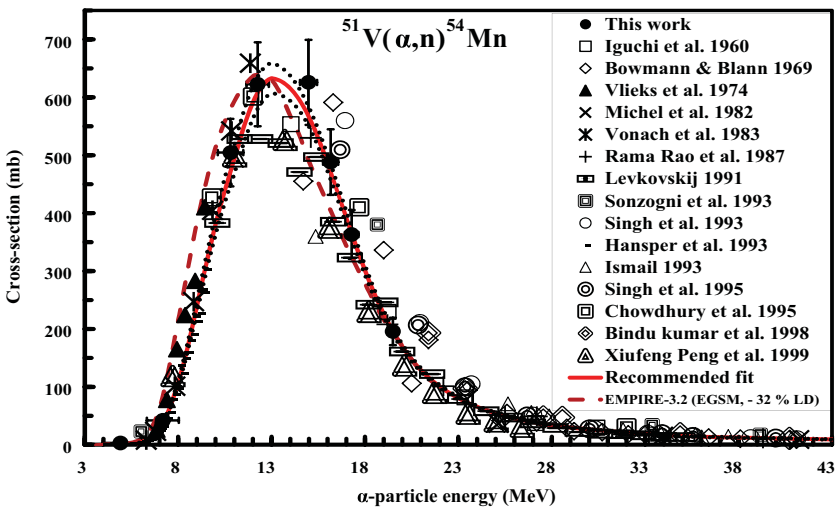

Figure 5. Recommended, theoretical and selected experimental excitation functions of $^{51}V(\alpha,n)^{54}Mn$ nuclear reaction. The black dotted lines are the 95% confidence of the fitting curve.

it. EMPIRE-3.1-calculated excitation function overestimates the experimental one except at the peak region, but have the same trend. Theoretical excitation functions based on EMPIRE-3.2.2 were calculated for various combinations of different parameters. We introduced here only the attempts that result in good agreement with the experimental data (figure 6).

We got the first consistence by performing the EMPIRE-3.2 default calculations, i.e. by means of the pre-equilibrium exciton model PCROSS using mean free path parameter value ($K_{mfp} = 1.05$) and the refitted (EGSM) model for the determination of the nuclear level densities. Changing the level density model to the refitted (GSM) model such that the level density parameter of ^{52}Mn decreased by 15% and using

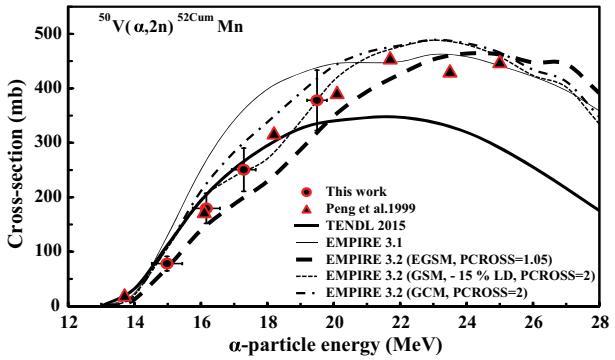

Figure 6. Experimental and theoretical excitation function of ^{50}V(α,2n)$^{52\text{-cum}}$Mn nuclear reaction.

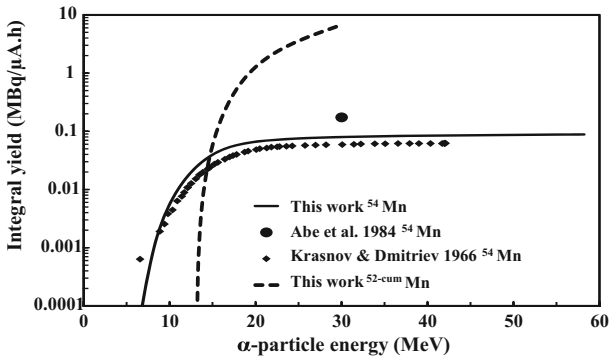

Figure 7. Integral yields of ^{54}Mn and ^{52}Mn production via α-particle-induced nuclear reaction on ^{nat}V.

mean free path value ($K_{mfp} = 2$) in the PCROSS model result in good agreement with the experimental data. The best agreement was achieved by changing the level density model to Gilbert and Cameron model from EMPIRE-2.18 (input data option in EMPIRE-3.2) and using mean free path value ($K_{mfp} = 2$) in the PCROSS model. Changing the level density model and the mean free path value in the PCROSS model affect obviously the excitation function in this reaction. This indicates the great contribution from pre-equilibrium emission. Both TENDL- and EMPIRE-displayed results represent cross-section of the (α,2n) channel only.

5. Integral yield

The integral yields for the production of the radionuclides ^{54}Mn and ^{52}Mn were calculated in (MBq/μA · h) using our calculated recommended excitation function for ^{54}Mn together with evaluated excitation function for $^{52\text{-cum}}$Mn and the stopping power/range of α-particles in ^{nat}V (figure 7).

The long-lived radionuclide ^{54}Mn recommended integral yield amounts to 0.09 MBq/μA · h in the energy range 58→5 MeV. The yield of ^{54}Mn production through ^{51}V(α,n) was measured experimentally in [27, 28]. The experimental value reported by Abe *et al* [27] was (4.7 μCi/μA · h) (0.17 MBq/μA · h) for 30 MeV α-particles. This is more than twice our presented value at the same energy range. The integral yield presented by Krasnov and Dmitriev [28] was about 0.06 MBq/μA · h in the energy range 42→6 MeV. Their result is about 26% lower than our calculated yield at the same energy range. The integral yield of ^{52}Mn was calculated using the available experimental excitation function, i.e. the present data and the data from [25]. The calculated yield for this radionuclide was about 6.7 MBq/μA · h in the energy range 30→13 MeV.

6. Conclusion

The excitation functions of α-particle-induced nuclear reactions on natural vanadium were measured using the stacked-foil activation technique and the ATOMKI cyclotron at the Institute for Nuclear Research, Debrecen, Hungary. The reactions ^{51}V(α,n)^{54}Mn and ^{50}V(α,2n)^{52}Mn have been studied from their threshold up to 20 MeV. Their excitation functions were compared with earlier experimental data found in the literature as well as theoretical data from the nuclear codes EMPIRE-3.1, EMPIRE-3.2.2 and TENDL 2015 library. The available experimental cross-section data in the literature are well established below and above the peak of the excitation function while the data in the peak region are scattered. Both EMPIRE and TENDEL predict the trend of the excitation function with different magnitudes. Good agreement between EMPIRE-3.2 excitation function and the experimental data for the (α,n) reaction was achieved using the EGSM level density model by decreasing the level density parameter of ^{54}Mn by 32%. Various combinations of level density models and mean free path parameters were consistent with experimental excitation function of the (α,2n) reaction.

Integral yields were calculated for the production of ^{54}Mn and ^{52}Mn. For the production of high-purity ^{54}Mn, we should decrease the production of the radionuclide ^{52}Mn and also the stable nuclide ^{53}Mn (produced via ^{51}V(α,2n), $E_{th} = 12.1$ MeV and ^{50}V(α,n), $E_{th} = 0.2$MeV). This can be achieved by using an energy window <12 MeV which prevents consideration of the competing channels ^{51}V(α,2n)^{53}Mn, ^{51}V(α,3n)^{52}Mn and ^{50}V(α,2n)^{52}Mn. The only remaining impurity is ^{53}Mn through the channel ^{50}V(α,n). However, due to the low abundance of ^{50}V, the contamination due to ^{53}Mn production will be very small. So using small-size cyclotrons and natural vanadium or enriched ^{51}V might be a convenient way to produce high-purity ^{54}Mn.

Acknowledgements

This work was supported and funded by Hungarian Scholarship Board through the Balassi Institute, Institute for Nuclear Research (ATOMKI), Hungarian Academy of Science and the Egyptian Academy of Scientific Research & Technology (ASRT). The authors acknowledge the staff and operators of Debrecen cyclotron for their help in performing irradiations. One of the authors (B M Ali) greatly appreciate the hospitality and support of the Institute for Nuclear Research (ATOMKI), Debrecen.

References

[1] A Lake Wooten, B C Lewis and S E Lapi, *Appl. Radiat. Isot.* **96**, 154 (2015)
[2] P E Johnson, G I Lykken and E D Korynta, *J. Nutr*. **121**, 711 (1991)
[3] A Takeda, S Ishwatorai and S Okada, *Brain Res.* **811**, 147 (1998)
[4] A Takeda, *Brain Res. Rev*. **41**, 79 (2003)
[5] M Klos, M Bartyzel and B Petelenz, *Nukleonika* **51**, 221 (2006)
[6] M Al-Abyad, M N H Comsan and S M Qaim, *Appl. Radiat. Isot.* **67**, 122 (2009)
[7] M Al-Abyad, I Spahn and S M Qaim, *Appl. Radiat. Isot.* **68**, 2393 (2010)
[8] A Hermanne, R Adam Rebeles, F Tárkányi, S Takács, M Takács and A Ignatyuk, *Nucl. Instrum. Methods B* **269**, 2563 (2011)
[9] F Ditrói, F Tárkányi, S Takács, A Hermanne, H Yamazaki, M Baba, A Mohammadi and A V Ignatyuk, *Nucl. Instrum. Methods B* **269**, 1878 (2011)
[10] M U Khandaker, H Haba, J Kanaya and N Otuka, *Nucl. Instrum. Methods B* **316**, 33 (2013)
[11] A Iguchi, H Amano and S Tanaka, *J. At. Energy Soc. Jpn* **2**, 682 (1960)
[12] W W Bowman and M Blann, *J. Nucl. Phys. A* **131**, 513 (1969)
[13] A E Vlieks, J F Morgan and S L Blatt, *J. Nucl. Phys. A* **224**, 492 (1974)
[14] R Michel, G Brinkmann and R Stuck, *Proceedings of the Antwerp Conference on Nuclear Data for Science and Technology* (Springer, Dordrecht, Netherlands, 1982) p. 599)
[15] H Vonach, R C Haight and G Winkler, *Phys. Rev. C* **28**, 2278 (1983)
[16] J Rama Rao, A V Mohan Rao, S Mukherjee, R Upadhyay, N L Singh, S Agarval, L Chaturvedi and P P Singh, *J. Phys. G* **13**, 535 (1987)
[17] V N Levkovskij, *Activation cross sections of average masses (A = 40–100) by protons and α-particles with average energies (E = 10–50 MeV)* (Inter Vesi, Moscow, USSR, 1991)
[18] A A Sonzogni, A S M A Romo, H O Mosca and S J Nassiff, *J. Radioanal. Nucl. Chem.* **170**, 143 (1993)
[19] N L Singh, S Agraval and J Rama Rao, *Can. J. Phys.* **71**, 115 (1993)
[20] V Y Hansper, A J Morton, S G Tims, C I W Tingwell, A F Scott and D G Sargood, *J. Nucl. Phys. A* **551**, 158 (1993)
[21] M Ismail, *Pramana – J. Phys*. **40**, 227 (1993)
[22] N L Singh, S Mukherjee, A V Mohan Rao, L Chaturvedi and P P Singh, *J. Phys. G* **21**, 399 (1995)
[23] D P Chowdhury, S Pal, S K Saha and S Gangadharan, *J. Nucl. Instrum. Methods B* **103**, 261 (1995)
[24] B Bindu Kumar, S Mukherjee and N L Singh, *Phys. Scr.* **57**, 201 (1998)
[25] X Peng, H Fuqing and X Long, *J. Nucl. Instrum. Methods B* **152**, 432 (1999)
[26] A Hermanne, R Adam Rebeles, F Tárkányi and S Takács, *Nucl. Instrum. Methods B* **356–357**, 28 (2015)
[27] K Abe, A Lizuka, A Hasegawa and S Morozumi, *J. Nucl. Mater*. **122–123**, 972 (1984)
[28] N N Krasnov and P P Dmitriev, *Atomnaya Energiya* **21**, 52 (1966)
[29] F Tárkányi, F Ditrói, S Takács, A Hermanne, M Baba and A V Ignatyuk, *Nucl. Instrum. Methods B* **269**, 1792 (2011)
[30] B M Ali, M Al-Abyad, U Seddik, S U El-Kameesy, F Ditrói, S Takács and F Tárkányi, *Nucl. Instrum. Methods B* **373**, 76 (2016)
[31] Z Kormány, *Nucl. Instrum. Methods A* **337**, 258 (1994)
[32] F Tárkányi, S Takács, K Gul, A Hermanne, M G Mustafa, M Nortier, P Oblozinsky, S M Qaim, B Scholten, Yu N Shubin and Z Youxiang, IAEA TECDOC-1211, Beam monitors reactions: charged particles cross-sections database for medical radioisotope production, Coordinated Research Project (IAEA, Vienna, 2001) pp. 77–80, available from: http://www.nds.iaea.org/medical (Updated version January 2007)
[33] J F Ziegler, M D Ziegler and J P Biersack, SRIM 2013 code, available from: http://srim.org
[34] G Székely, *Comput. Phys. Commun*. **34**, 313 (1985)
[35] National Nuclear Data Center, Brookhaven National Laboratory, NuDat 2.6 database, available from: http://www.nndc.bnl.gov/hbin/nudat
[36] ISO, Guide to expression of uncertainty in measurement, ISBN 92-67-10188-9 (International Organization for Standardization, Geneva, 1995)
[37] M Herman, R Capote, M Sin, A Trkov, B V Carlson, P Obložinský, C M Mattoon, H Wienke, S Hoblit, C Young-Sik, V Plujko and V Zerkin, EMPIRE-3.1 Rivoli: Modular system for nuclear reaction calculations and nuclear data evaluation; User's Manual (2012)
[38] M Herman, R Capote, M Sin, A Trkov, B V Carlson, P Obložinský, C M Mattoon, H Wienke, S Hoblit, C Young-Sik, G P A Nobre, V A Plujko and V Zerkin, EMPIRE-3.2 Malta: Modular system for nuclear reaction calculations and nuclear data evaluation; User's Manual (2013)

[39] A J Koning, S Hilaire and S Goriely, TALYS-1.6: A nuclear reaction program, Nuclear Research and Consultancy Group (NRG) (2013)
[40] M N Aslam and S M Qaim, *Appl. Radiat. Isot.* **89**, 65 (2014)
[41] B M Ali, M Al-Abyad, U Seddik, S U El-Kameesy, F Ditrói, S Takács and F Tárkányi, *Nucl. Instrum. Methods B* **321**, 30 (2014)
[42] A Ssyed, A Elbinawi, M Al-Abyad, U Seddik and I I Bashter, *Pramana – J. Phys.* **84**, 569 (2015)
[43] IAEA-CRP, Reference Input Parameter Library (RIPL), IAEA-TECDOC-1034, Vienna (1998), http://www-nds.iaea.org/RIPL-3/
[44] A J Koning, D Rochman, J Kopecky, J Ch Sublet, M Fleming, E Bauge, S Hilaire, P Romain, B Morillon, H Duarte, S van der Marck, S Pomp, H Sjostrand, R Forrest, H Henriksson, O Cabellos, S Goriely, J Leppanen, H Leeb, A Plompen and R Mills, TENDL-2015: TALYS-based evaluated nuclear data library (2016)
[45] Table curve: 2d-Automated curve fitting analysis, Systat Software Inc, available from: www.sigmaplot.co.uk/products/tablecurve2d/tablecurve2d.php